Optimization of graphene-based quantum Hall arrays for recursive star-mesh transformations

D. S. Scaletta,[1] S. M. Mhatre,[2] N. T. M. Tran,[2,3] C. H. Yang,[2,4] H. M. Hill,[2] Y. Yang,[5] L. Meng,[5] A. R. Panna,[2] S. U. Payagala,[2] R. E. Elmquist,[2] D. G. Jarrett,[2] D. B. Newell,[2] and A. F. Rigosi[2,a)]

[1]*Department of Physics, Mount San Jacinto College, Menifee, California 92584, USA*

[2]*Physical Measurement Laboratory, National Institute of Standards and Technology (NIST), Gaithersburg, Maryland 20899, USA*

[3]*Joint Quantum Institute, University of Maryland, College Park, Maryland 20742, USA*

[4]*Graduate Institute of Applied Physics, National Taiwan University, Taipei, 10617, Taiwan*

[5]*Graphene Waves, LLC, Gaithersburg, Maryland 20878, USA*

A mathematical approach is adopted for optimizing the number of total device elements required for obtaining high effective quantized resistances in graphene-based quantum Hall array devices. This work explores an analytical extension to the use of star-mesh transformations such that fractal-like, or recursive, device designs can yield high enough resistances (like 1 EΩ, arguably the highest resistance with meaningful applicability) while still being feasible to build with modern fabrication techniques. Epitaxial graphene elements are tested, whose quantized Hall resistance at the $\nu = 2$ plateau ($R_{\mathrm{H}} \approx 12906.4\ \Omega$) becomes the building block for larger effective, quantized resistances. It is demonstrated that, mathematically, one would not need more than 200 elements to achieve the highest pertinent resistances.

a) Author to whom correspondence should be addressed. email: afr1@nist.gov

Graphene has been the subject of extensive research over the past decade due to its remarkable optical and electrical properties [1-4]. Epitaxial graphene (EG), grown on 4H-SiC in the case of this work, has been developed into devices for electrical metrology due to its robust quantum Hall effect (QHE) across a wide range of magnetic fields (B-fields). For these devices to be successfully implemented as standards, the exhibited resistance must be well-quantized [5-10]. Devices made from EG display quantized Hall resistance values of $\frac{1}{(4m+2)}\frac{h}{e^2}$, where m is an integer, h is the Planck constant, and e is the elementary charge. Most EG-based devices that are used as resistance standards operate at the resistance plateau formed by the $\nu = 2$ Landau level ($R_{\mathrm{H}} = \frac{1}{2}\frac{h}{e^2} \approx 12906.4037\ \Omega$) [11-15], with other efforts using the $\nu = 6$ plateau [16].

This common single-value constraint severely limits the infrastructure and equipment with which one may disseminate the unit of the ohm. Two dominant types of efforts to transcend these limitations include the use of quantum Hall array resistance standards (QHARS) to link multiple Hall elements in parallel or series and the use of p-n junctions, with both approaches yielding resistances of qR_{H} where q is a positive rational number [17-28].

One of the limiting factors in QHARS development is the total area of high-quality EG, currently limited to the centimeter scale [29]. Other device design alternatives must be explored since these growth limitations restrict the total number of feasibly attainable QHARS elements. For instance, the maximum achievable quantized resistance from having 500 elements in series is approximately 6.5 MΩ, which is much smaller than the range of resistances currently calibrated globally – up to PΩ levels in some cases [30].

Recently, EG-based QHARS devices were used in experimental configurations enabling the application of the mathematical star-mesh transformation [31]. And though that approach can scale up to higher resistances [30, 32-34], such limits of applicability of star-mesh transformations have not yet been explored. For that reason, this work explores a framework for utilizing star-mesh QHARS device designs in a recursive manner to minimize the required number of array elements for very high effective quantized resistances. Example data from QHARS devices are also shown to support the underlying principles of this work. Given that this formulation is independent of the material's properties, it may be applied to other material systems that exhibit the QHE, as well as artifact standard resistors.

Devices were prepared in the same Si sublimation procedure described in Ref. [31] and in three major steps: (1) growth, (2) fabrication, (3) post-fabrication and packaging. Grown EG films were inspected using optical and confocal laser scanning microscopy [36], followed by fabrication of device contacts composed of NbTiN [29, 37]. Gateless control of the EG

electron density for some devices was also implemented via functionalization with $Cr(CO)_3$ [38-40]. Devices were measured in a cryostat at 2 K with a Dual Source Bridge (DSB) [31].

Some of the fundamentals of star-mesh transformations are well-summarized in early work [41-42], and the framework presented herein begins by inspecting two resistance networks containing *N* terminals, like those shown in left and right columns of Fig. 1. One may then derive a mathematical relationship between a star network (where all arms meet at a central node as in the left column of Fig. 1) and its equivalent mesh network (*N* is equal in both networks, but the mesh contains one fewer node):

$$R_{ij} = R_i R_j \sum_{\alpha=i}^{N} \frac{1}{R_\alpha} \tag{1}$$

In Eq. 1, the indices go as high as *N* with the condition that $i \neq j$. To simplify how a QHARS device undergoes minimal-element design optimization, let us define $q \equiv \frac{R}{R_H}$, where q is defined as the number of single Hall elements held at the $\nu = 2$ plateau to obtain the total resistance *R*. This number has been characterized as the *coefficient of effective resistance* (CER) in other work related to graphene-based devices [43-44], with the key difference being that, for this work, functions of q may be presented as analytical, wherein such functions will be easier to manage as mathematical objects than a discretized set. It should be noted that this coefficient q, when applied to the development of actual device designs, must be restricted to the set of positive integers ($q: q \in \mathbb{Z}^+$).

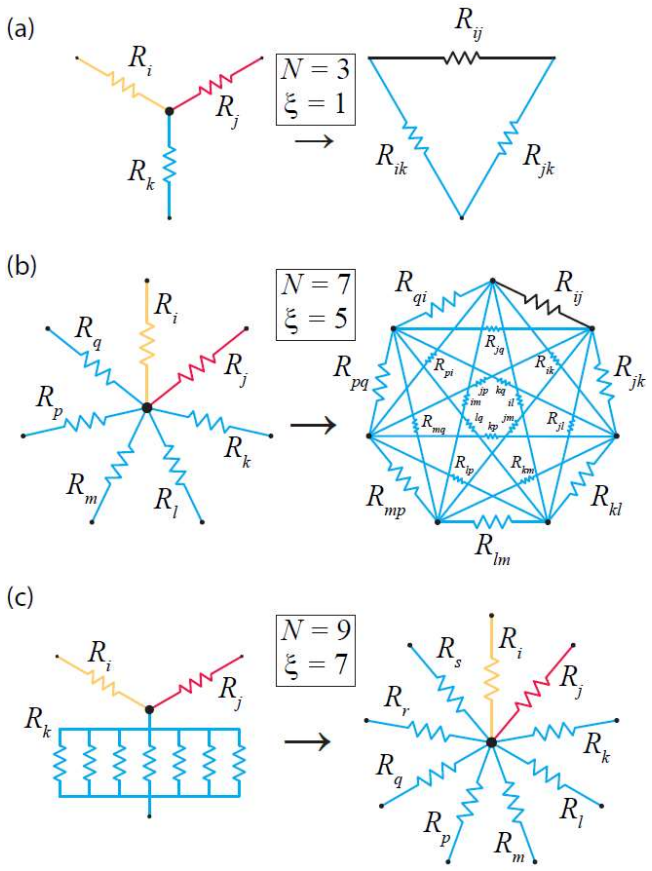

FIG. 1. Various star-mesh transformations are shown with the stars on the left and the meshes on the right (except for (c)), with N and ξ defined as the number of terminals and number of electrically grounded branches, respectively. (a) A Y-Δ transformation ($N = 3$). (b) A star-mesh transformation ($N = 9$). (c) Equivalence between a Y network containing a parallel set of electrically grounded elements and a star network with the same number of independent, single-element branches as there are parallel elements. The yellow and red branches represent the two primary terminals for measuring high quantized resistances.

In an experimental context, measurements are generally performed across two of the branches of a Y-Δ network, with the third branch being electrically grounded [31]. Since experimental setups only employ a high and low voltage terminal (two terminals), a reasonable condition to introduce is that all other existing terminals be grounded since future measurements of such networks would require this. Illustrations of various star-mesh transformations are shown in Fig. 1, where one defines ξ as the number of grounded branches. Though this number is always two less than N, it is still useful to designate for subsequent mathematical manipulation. It should be noted that a Y network containing a parallel set of

grounded elements is topologically equivalent to a star network with the same number of independent, single-element branches as there are parallel elements, where the ξ branches are all grounded to the same point. Therefore, the lowest number of elements any branch may contain is 1. The final two quantities to define are D_T, or total number of elements in a QHARS device, and M, a recursion factor that will be detailed later. The objective of optimization is to substantially reduce the total required elements to develop QHARS devices with quantized resistances well beyond the MΩ level. With the earlier definition normalizing quantized resistances, one may rewrite Eq. (1) as the following expression:

$$q_{ij} = q_i q_j \sum_{\alpha=i}^{N} \frac{1}{q_\alpha} \tag{2}$$

Next, focusing exclusively on the Y-Δ configuration for simplicity (where ξ = 1), the number of actual elements (q with a single index) required to enable the measurement of a much larger, "effective", number of elements (q with two indices) yields the expression of the abstract quantity q_{ij} (recall from earlier that mesh resistors are virtual, not physical):

$$q_{ij} = q_i + q_j + \frac{q_i q_j}{q_k} \tag{3}$$

In order to maximize the effective CER in Eq. 3 (q_{ij}), let us impose the previously held condition that $q_k = 1$:

$$q_{ij} = q_i + q_j + q_i q_j \tag{4}$$

Since Eq. 4 can yield many high CERs due to the multiplication term, one can optimize device designs by finding the global minimum of this function of q_i and q_j that yields the desired q_{ij} (which is treated as a constant, to be selected by the designer). This minimization problem may be solved with straightforward substitution and derivatives, where one temporarily defines the sum of the QHR elements in the two relevant branches to be $\alpha \equiv q_i + q_j$ (one need not include q_k, which has already been set to 1). Rewriting Eq. 4 in terms of α and q_i (the latter being arbitrarily selected), one gets:

$$\alpha = \frac{q_{ij} + {q_i}^2}{q_i + 1} \tag{5}$$

And through conventional extraction of neighborhood extrema:

$$\frac{d\alpha}{dq_i} = \frac{{q_i}^2 + 2q_i - q_{ij}}{(q_i + 1)^2} = 0$$

(6)

The positive root of Eq. 6 yields:

$$q_i = \sqrt{q_{ij} + 1} - 1$$

(7)

This solution for q_i also applies to q_j given the symmetry of Eq. 4. One final check to this analysis may be computed and verified: $\frac{d^2\alpha}{dq_i^2} > 0$. This second derivative result verifies that Eq. 7 is, in fact, a global minimum and not a global maximum (global rather than local since the domain of q is non-negative). To extend this analysis to the general star-mesh case, suppose there are *N* terminals:

$$q_{ij} = q_i + q_j + \frac{q_i q_j}{q_k} + \frac{q_i q_j}{q_l} + \frac{q_i q_j}{q_m} + \cdots \frac{q_i q_j}{q_N}$$

(8)

And again, the ξ branches have $q_k = q_l = q_m = \cdots = q_N = 1$:

$$q_{ij} = q_i + q_j + \xi q_i q_j$$

(9)

Equation 9, where $N = \xi + 2$, appears similar to Eq. 4, and by repeating the previous procedure:

$$q_i = \frac{1}{\xi}\sqrt{\xi q_{ij} + 1} - 1 = \frac{1}{N-2}\sqrt{(N-2)q_{ij} + 1} - 1$$

(10)

Equation 10 shows the generalized case solution for determining the CER where *N* terminals are used. The total number of elements in the entire device may then be written: $D_T = 2q_i + \xi$. With this analysis, one may use example values of R_{ij} (1 EΩ, 1 PΩ, 1 TΩ, 1 GΩ) to calculate the minimum number of required elements for those values, as in Fig. 2. Solutions (q_i) found for each value must be rounded to the nearest integer before calculating D_T. And the error introduced from rounding may be represented as deviations from the nominal example values (specifically, as $Dev = \frac{q_{ij}^{(rounded)}}{q_{ij}^{(nominal)}} - 1$). Both the deviations and D_T are plotted as a function of ξ in Fig. 2.

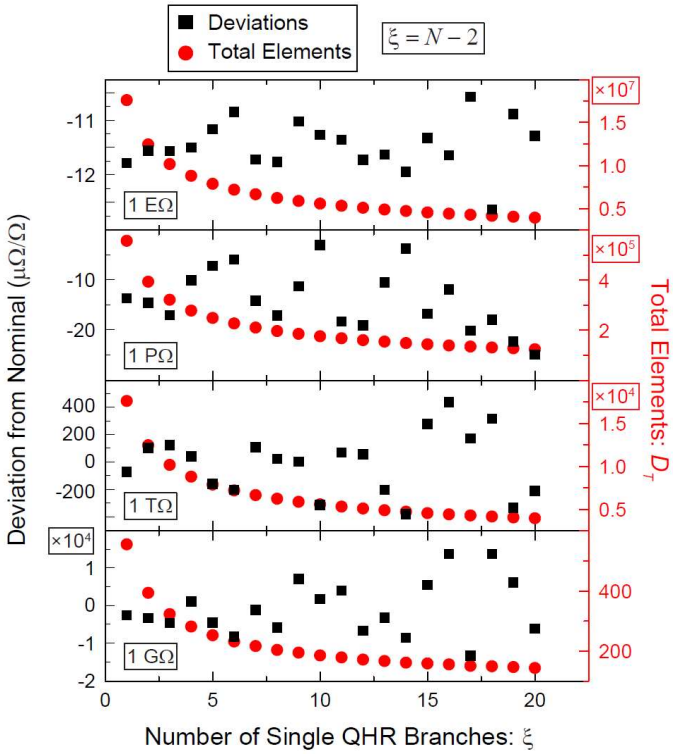

FIG. 2. Example values of high effective resistances are used to calculate the minimum number of required elements for such values (red, right side vertical axis) as well as the deviations of those hypothetical QHARS devices from the nominal example values (1 EΩ, 1 PΩ, 1 TΩ, 1 GΩ – black, left side vertical axis). The horizontal axis counts the number of single QHR branches (ξ) as a proxy for the star-mesh configuration used in the calculation.

The calculated deviations do not prevent these hypothetical QHARS devices from being useful, as many specialized Wheatstone bridges can operate without an exact decade value of resistance [31]. Though this optimization process reduced D_T for GΩ level resistances to reasonable numbers for fabrication, those numbers are still high for larger resistors (in the millions for 1 EΩ). Therefore, one may expand on this optimization process by adopting recursive star-mesh designs that resemble the construction of some kinds of fractals.

Implementing a recursive treatment to star-mesh QHARS device designs may vastly expand the availability of quantized resistances. For instance, Fig. 3 summarizes a few cases in which recursive features have been included, such as embedding Y-Δ networks within Y-Δ networks. A new parameter can be designated to characterize this recursion: M. With a desired resistance selected, one may expand q_{ij} into a star network (with all ξ branches valued as $q = 1$ and grounded). Every

subsequent expansion of all non-grounded elements increases the characteristic recursion factor M by one. For Fig. 3 (a)-(d), the Y-Δ networks is analyzed, whereas in Fig. 3 (e)-(h), more complex cases like the 4-terminal ($N = 4$, or equivalently $\xi = 2$, as defined earlier) and the 7-terminal ($N = 7$, or equivalently $\xi = 5$) configurations are analyzed. The complexity of the latter two cases warrants a change in representation to topologically equivalent, more abstract diagrams of device configurations.

To account for the addition of this new parameter M, the subscripts will be modified so as to not alter previously adopted notation; that is, actual elements represented by $q_{M:i}$ (single index) and effective number of elements represented by $q_{M:ij}$ (two indices). By repeating the optimization process in the previous section with all intermediate resistors fully expanded, leaving the QHARS device in its final configuration of elements, one obtains the actual number of elements needed per non-grounded sub-branch:

$$q_{M:i} = \frac{1}{\xi}\left(\xi q_{M:ij} + 1\right)^{2^{-M}} - \frac{1}{\xi} \tag{11}$$

With this information, one can count the total number of elements in the final QHARS device:

$$D_T\left(M, \xi, q_{M:ij}\right) = 2^M q_{M:i} + \sum_{x=1}^{M} 2^{x-1}\xi = \frac{2^M}{\xi}\left(\xi q_{M:ij} + 1\right)^{2^{-M}} - \frac{2^M}{\xi} + (2^M - 1)\xi \tag{12}$$

This function of three variables may now serve as the starting point for a final optimization process.

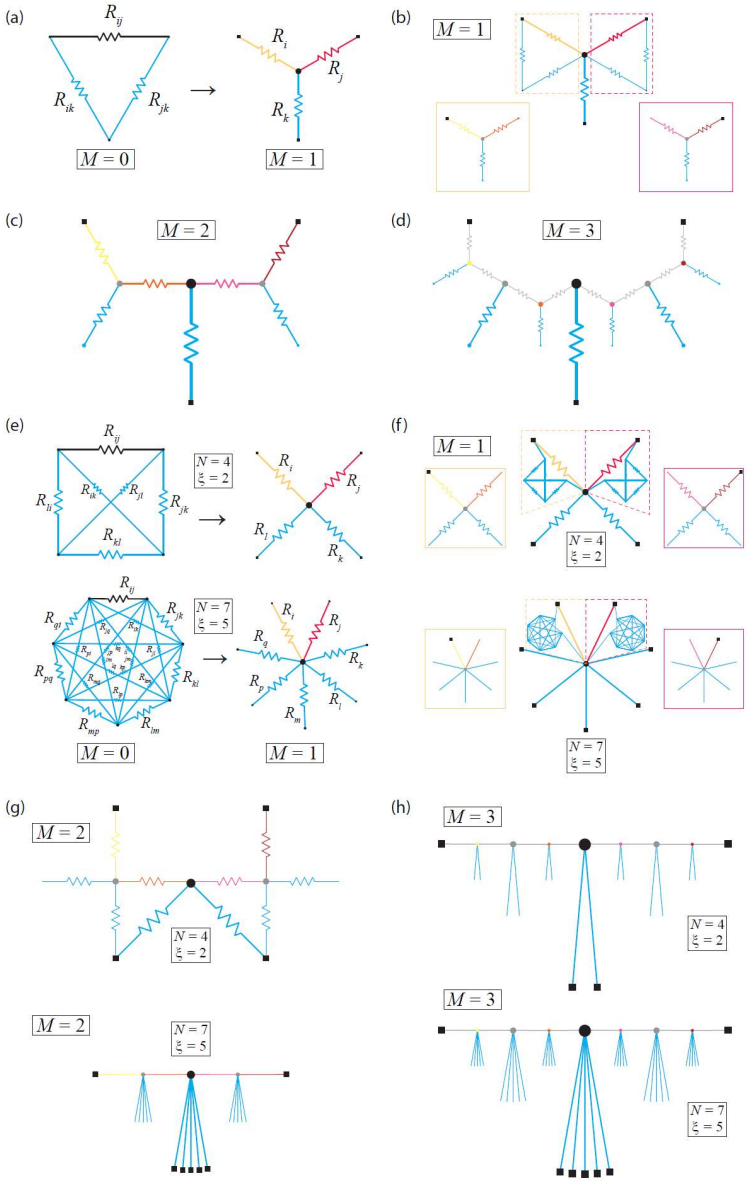

FIG. 3. (a) R_{ij} (equivalently, q_{ij}) as a Y-Δ network. Every subsequent expansion of all non-grounded elements increases the characteristic recursion factor M by one. (b) Every resistor in the non-grounded path is expanded as a Y-Δ network, with the next substitution shown in (c). (d) A third recursion is applied to all non-grounded resistors. (e) A diagram similar to (a) is produced for 4-terminal (or $N = 4$, equivalently represented in the derivation as $\xi = 2$, the number of grounded branches) and 7-terminal (or $N = 7$, equivalently represented in the derivation as $\xi = 5$, the number of grounded branches) star-mesh networks. (f) Like (b), every resistor in the non-grounded path is expanded as a network of the same number of terminals, with the next substitution shown in (g). (g) Like (c), this diagram shows the next

iteration ($M = 2$) of the recursion for both the 4-terminal (top) and 7-terminal (bottom) cases. Note that the top and bottom appear different in drawing format. This topologically equivalent diagram of the device configurations must be used due to the added difficulty of drawing more complex meshes with each recursive iteration. (h) Like (d), this diagram shows the next iteration ($M = 3$) of the recursion for the two cases ($N = 4$ and $N = 7$).

As per the construction of Eq. 12, it would benefit the designer to first select a desired final element count $q_{M:ij}$ (proxy for resistance). For the sake of example, the upper bound on arguably useful resistances for metrology is selected: 1 EΩ ($q_{M:ij} \approx 7.74809 \times 10^{13}$).

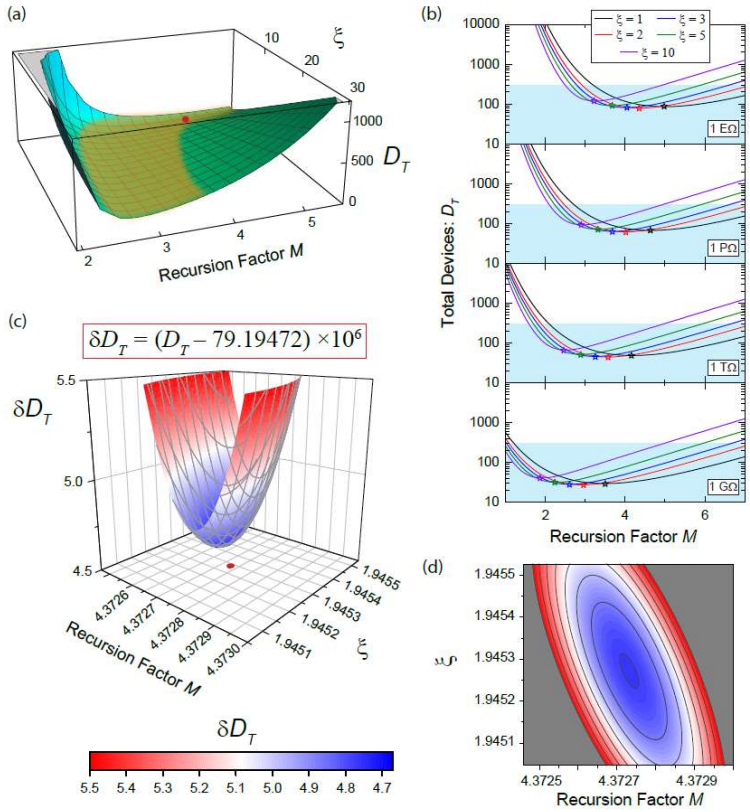

FIG. 4. (a) D_T is plotted as a function of ξ and M, while fixing $q_{M:ij}$ corresponding to 1 EΩ. The minimum is marked as a red spot, and the shaded orange region refers to the embankment of practically feasible design solutions in the text. (b) The behavior of D_T as a function of M at various fixed values of ξ. D_T is plotted for values of $q_{M:ij}$ corresponding to 1 PΩ, 1 TΩ, and 1 GΩ. Shaded cyan regions indicate an upper bound of 300 elements, a rough approximation for fabrication capabilities. Every curve has its minimum marked by a star. (c) Magnification of global minimum of D_T according to the listed transformation. A corresponding contour projection is shown in (d).

Attempting to analytically find the minimum of this now two-variable function quickly reveals that one must solve a large order polynomial, and since such large polynomials are not guaranteed to have closed-form solutions (see SM), finding the global minimum must be done numerically. Fixing $q_{M:ij}$ to correspond to 1 EΩ, one may plot this function as seen in Fig. 4 (a). The global minimum is marked as a red spot and can be greatly magnified to see the subtle approach to that extremum (see Fig. 4 (c) and (d)). Inspecting this solution space yields two observations. First, there is some flexibility in how to design a device since there are a set of solutions with low D_T along the embankment region of M = 3 and ξ = 2 to 4 (shaded orange in Fig. 4 (a)). The embankment is also presented in Fig. 4 (b), where semi-logarithmic curves for D_T are plotted for fixed values of ξ (and for 1 EΩ, 1 PΩ, 1 TΩ, and 1 GΩ). Shaded cyan regions indicate an upper bound of 300 elements, which is a rough approximation for what is likely within fabrication capabilities [28]. The reason one should take note of this cyan region is because exclusively using the global minimum, when accounting for fact that one must use integers in practice, may not give a nominal resistance value close enough to the desired value, as defined by the experimenter (see SM for example calculations).

Generally, optimal configurations using high recursion make it inflexible to achieve an exact desired value with a low error. What can be learned by calculating example device designs is that the likelihood of obtaining a resistance close to a desired value is statistically greater when M is taken to be 2 or 3 since the embankment region in Fig. 4 (a) allows for greater flexibility in ξ (and thus more chances at obtaining a combination of parameters yielding an optimally accurate resistance). See the SM for more details.

With greater flexibility in QHARS designing, one may now more closely analyze the extent to which such flexibility can improve nominal value accuracy. For this analysis, M = 3 (initially) since M = 4 too greatly restricts the parameter space. With a chosen $q_{3:ij}$, D_T can be minimized in terms of ξ. This minimization can be seen in Fig. 5 (a) on the red vertical axis (D_T). Naturally, one selects an integer ξ such that D_T is minimized and proceeds to obtain $q_{3:i}$. As done in the SM, deviations of the final device design may be calculated (represented as black squares in Fig. 5 (a)). Furthermore, rounding to the closest integer may not always yield the optimal deviation, as seen in the 1 GΩ case, where the optimal ξ yields a resistance, whose deviation falls off-scale. Therefore, it may be fitting to perturb the solution of integer parameters to see if more optimal solutions exist. Such perturbations are also shown in Fig. 5 (a) as black hollow triangles, indicating that better accuracies are available at limited increases in D_T. These more optimal parameters are rendered into QHARS device designs in the SM.

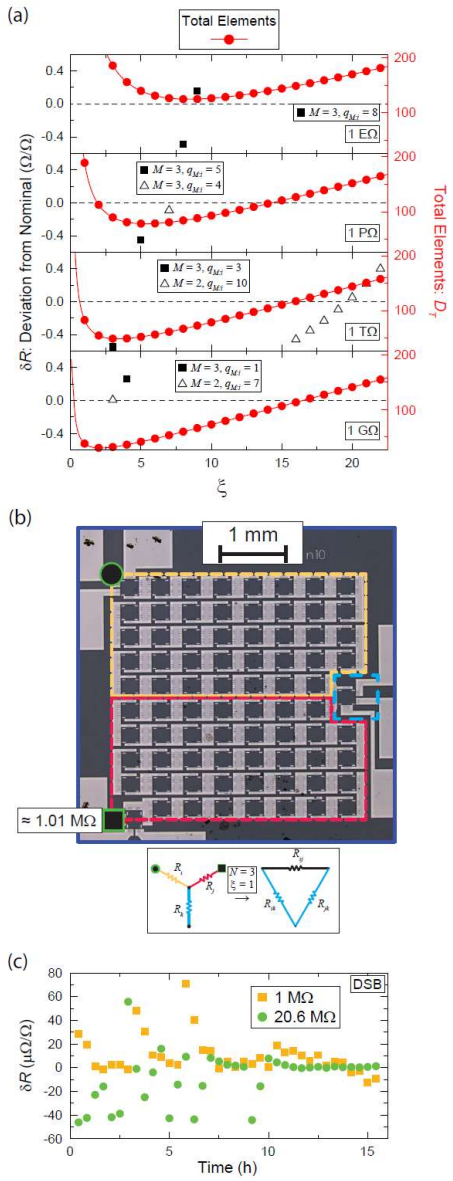

FIG. 5. (a) With $q_{3:ij}$ chosen, D_T can be minimized in terms of ξ on the red vertical axis. Deviations of the final device design may be calculated from the solutions closest to the minima when rounded to integers (represented as black squares). When solutions are perturbed by alternative means of rounding to an integer (like alternating rounding down and up for the relevant parameters), possible improvements may be found to the accuracy of the resistance output when compared to the desired resistance (black, hollow triangles). (b) An example image of a device valued nominally at about 1 MΩ due to its 78 devices in series, with a middle element on the right side, center, as the grounded branch. Accompanying illustration shows the corresponding diagramatic representation of the Y-Δ transformation ($N = 3$). (c) Example measurement of a QHARS device using a DSB, both across its full array (gold) and in the Y-Δ configuration (green).

To test these concepts, several device measurements were performed on a symmetric Y-Δ network. A DSB was used, as in Ref. [31], to more precisely measure the output resistances of one type of QHARS (see SM) in Fig. 5 (b), where the offsets from nominal for the values 1 MΩ and 20.6 MΩ were 1812.6 Ω and 6699.473 Ω, respectively. The demonstration of the device's ability to be used in a star-mesh network makes it evident that this mathematical transformation has the promise of substantially reducing the complexity of future QHARS devices, especially those in use for electrical metrology.

In conclusion, a mathematical approach was adopted for optimizing the number of total elements required for obtaining high effective quantized resistances in graphene-based quantum Hall array devices. Star-mesh transformations involving recursive device designs yielded resistances as high as nearly 1 EΩ. Furthermore, designs may be lightly modified to enhance accuracy to a desired value while still remaining feasible to build with modern fabrication techniques. A general observation based on the results suggests that using fewer recursions would allow the greatest flexibility in device design, including designs that are not wholly symmetric in their star-mesh branches as treated in this work. Lastly, these designs are encouraged to be tested for their promise in removing the need for artifact resistors and for providing access to the quantum SI without the need for a lengthy calibration chain.

SUPPLEMENTARY MATERIAL

The Supplementary Material includes additional mathematical details, calculations for showing deviations from nominal resistances, examples of other device designs, and QHARS devices used in experiments.

ACKNOWLEDGMENTS

The work of C.H.Y. and S.M.M. at NIST was made possible by C.-T. Liang of National Taiwan University, and the authors thank him for this endeavor. The authors would like to express thanks to T. Mai, F. Fei, G. J. Fitzpatrick, and E. C. Benck for their assistance in the NIST internal review process.

The authors declare no competing interests. Commercial equipment, instruments, and materials are identified in this paper in order to specify the experimental procedure adequately. Such identification is not intended to imply recommendation or endorsement by the National Institute of Standards and Technology or the United States government, nor is it intended to imply that the materials or equipment identified are necessarily the best available for the purpose.

REFERENCES

[1]A.K. Geim and K.S. Novoselov, Nat. Mater. **6**, 183 (2007).

[2]A.H. Castro Neto, F. Guinea, N. M. R. Peres, K. S. Novoselov, and A. K. Geim, The electronic properties of graphene. Rev. Mod. Phys. **81**, 109 (2009).

[3] S. Das Sarma, S. Adam, E.H. Hwang, and E. Rossi, Electronic transport in two-dimensional graphene. Rev. Mod. Phys. **83**, 407 (2011).

[4] K.S. Novoselov, V.I. Fal'ko, L. Colombo, P.R. Gellert, M.G. Schwab, and K. A. Kim, A roadmap for graphene. Nature **490**, 192 (2012).

[5] R. Ribeiro-Palau, F. Lafont, J. Brun-Picard, D. Kazazis, A. Michon, F. Cheynis, O. Couturaud, C. Consejo, B. Jouault, W. Poirier, and F. Schopfer, Quantum Hall resistance standard in graphene devices under relaxed experimental conditions. Nature Nanotechnol. **10**, 965 (2015).

[6] T. Oe, A.F. Rigosi, M. Kruskopf, B.-Y. Wu, H.-Y. Lee, Y. Yang, R.E. Elmquist, N.-H. Kaneko, D.G. Jarrett, Comparison between NIST graphene and AIST GaAs quantized Hall devices. IEEE Trans. Instrum. Meas. **69**, 3103-3108, (2019).

[7] A. F. Rigosi, R. E. Elmquist, The quantum Hall effect in the era of the new SI. Semicond. Sci. Technol. **34**, 093004 (2019).

[8] A. Tzalenchuk, S. Lara-Avila, A. Kalaboukhov, S. Paolillo, M. Syväjärvi, R. Yakimova, O. Kazakova, T.J.B.M. Janssen, V. Fal'ko, and S. Kubatkin, Towards a quantum resistance standard based on epitaxial graphene. Nat Nanotechnol. **5**, 186 (2010).

[9] H. He, S. Lara-Avila, T. Bergsten, G. Eklund, K. H. Kim, R. Yakimova, Y. W. Park, S. Kubatkin, Stable and tunable charge carrier control of graphene for quantum resistance metrology. Conference on Precision Electromagnetic Measurements (CPEM 2018) 1-2 (2018).

[10] B. Jeckelmann, B. Jeanneret, The quantum Hall effect as an electrical resistance standard. Rep. Prog. Phys. **64**, 1603 (2001).

[11] T.J.B.M. Janssen, A. Tzalenchuk, R. Yakimova, S. Kubatkin, S. Lara-Avila, S. Kopylov, and V.I. Fal'ko, Anomalously strong pinning of the filling factor v=2 in epitaxial graphene. Phys Rev B **83**, 233402 (2011).

[12] A.F. Rigosi, C.-I. Liu N.R. Glavin, Y. Yang, H.M. Hill, J. Hu, A.R. Hight Walker, C.A. Richter, R.E. Elmquist, and D.B. Newell, Electrical stabilization of surface resistivity in epitaxial graphene systems by amorphous boron nitride encapsulation. ACS Omega **2**, 2326 (2017).

[13] M. Kruskopf, S. Bauer, Y. Pimsut, A. Chatterjee, D. K. Patel, A. F. Rigosi, R. E. Elmquist, K. Pierz, E. Pesel, M. Götz, J. Schurr, Graphene quantum Hall effect devices for AC and DC electrical metrology. IEEE Trans. Electron Dev. **68**, 3672, (2021).

[14] M. Marzano, M. Kruskopf, A. R. Panna, A. F. Rigosi, D. K. Patel, H. Jin, S. Cular, L. Callegaro, R. E. Elmquist, M. Ortolano, Implementation of a graphene quantum Hall Kelvin bridge-on-a-chip for resistance calibrations. Metrologia **57**, 015007 (2020).

[15] A.F. Rigosi, A.R. Panna, S.U. Payagala, M. Kruskopf, M.E. Kraft, G.R. Jones, B.-Y. Wu, H.-Y. Lee, Y. Yang, J. Hu, D.G. Jarrett, D.B. Newell, R.E. Elmquist, Graphene devices for tabletop and high-current quantized Hall resistance standards. IEEE Trans. Instrum. Meas. **68**, 1870 (2019).

[16] A. R. Panna, I-F. Hu, M. Kruskopf, D. K. Patel, D. G. Jarrett, C.-I Liu, S. U. Payagala, D. Saha, A. F. Rigosi, D. B. Newell, C.-T. Liang, R. E. Elmquist, Graphene quantum Hall effect parallel resistance arrays. Phys. Rev. B **103**, 075408 (2021).

[17] J. Hu, A.F. Rigosi, M. Kruskopf, Y. Yang, B.-Y. Wu, J. Tian, A.R. Panna, H.-Y. Lee, S.U. Payagala, G.R. Jones, M.E. Kraft, D.G. Jarrett, K. Watanabe, T. Taniguchi, R.E. Elmquist, and D.B. Newell, Towards epitaxial graphene pn junctions as electrically programmable quantum resistance standards. Sci. Rep. **8**, 15018 (2018).

[18] S. Novikov, N. Lebedeva, J. Hamalainen, I. Iisakka, P. Immonen, A. J. Manninen, and A. Satrapinski, Mini array of quantum Hall devices based on epitaxial graphene. J. Appl. Phys. **119**, 174504 (2016).

[19] F. Delahaye, Series and parallel connection of multiterminal quantum Hall-effect devices. J. Appl. Phys. **73**, 7914 (1993).

[20] J. Hu, A.F. Rigosi, J.U. Lee, H.-Y. Lee, Y. Yang, C.-I. Liu, R.E. Elmquist, and D.B. Newell, Quantum transport in graphene p-n junctions with moiré superlattice modulation. Phys. Rev. B **98**, 045412 (2018).

[21] M. Woszczyna, M. Friedmann, T. Dziomba, T. Weimann, and F.J. Ahlers, Graphene pn junction arrays as quantum-Hall resistance standards. Appl. Phys. Lett. **99**, 022112 (2011).

[22] D. Patel, M. Marzano, C.-I Liu, H. M. Hill, M. Kruskopf, H. Jin, J. Hu, D. B. Newell, C.-T. Liang, R. Elmquist, A. F. Rigosi, Accessing ratios of quantized resistances in graphene p–n junction devices using multiple terminals. AIP Adv. **10**, 025112 (2020).

[23] Z. S. Momtaz, S. Heun, G. Biasiol, S. Roddaro, Cascaded Quantum Hall Bisection and Applications to Quantum Metrology. Phys. Rev. Appl. **14**, 024059 (2020).

[24] J. Park, W. S. Kim, Realization of 5h/e^2 with graphene quantum Hall resistance array. Appl. Phys. Lett. **116**, 093102 (2020).

[25] A. Lartsev, S. Lara-Avila, A. Danilov, S. Kubatkin, A. Tzalenchuk, and R. Yakimova, A prototype of RK/200 quantum Hall array resistance standard on epitaxial graphene. J. Appl. Phys. **118**, 044506 (2015).

[26] D. H. Chae, M. S. Kim, T. Oe, N. H. Kaneko, Series connection of quantum Hall resistance array and programmable Josephson voltage standard for current generation at one microampere. Metrologia **59**, 065011 (2022).

[27] S. M. Mhatre, N. T. M. Tran, H. M. Hill, C.-C. Yeh, D. Saha, D. B. Newell, A. R. Hight Walker, C.-T. Liang, R. E. Elmquist, A. F. Rigosi, Versatility of uniformly doped graphene quantum Hall arrays in series. AIP Adv. **12**, 085113 (2022).

[28] H. He, K. Cedergren, N. Shetty, S. Lara-Avila, S. Kubatkin, T. Bergsten, G. Eklund, Accurate graphene quantum Hall arrays for the new International System of Units. Nat. Commun. **13**, 6933 (2022).

[29] M. Kruskopf, A. F. Rigosi, A. R. Panna, M. Marzano, D. K. Patel, H. Jin, D. B. Newell, and R. E. Elmquist, Two-terminal and multi-terminal designs for next-generation quantized Hall resistance standards: contact material and geometry. IEEE Trans. Electron Dev. **66**, 3973 (2019).

[30] K. M. Yu, D. G. Jarrett, A. F. Rigosi, S. U. Payagala and M. E. Kraft, Comparison of Multiple Methods for Obtaining PΩ Resistances with Low Uncertainties. IEEE Trans. Instrum. Meas. **69**, 3729-3738 (2020).

[31] D. G. Jarrett, C.-C. Yeh, S. U. Payagala, A. R. Panna, Y. Yang, L. Meng, S. M. Mhatre, N. T. M. Tran, H. M. Hill, D. Saha, R. E. Elmquist, D. B. Newell, A. F. Rigosi, Graphene-Based Star-Mesh Resistance Networks. IEEE Trans. Instrum. Meas. **70**, XXXX (2023).

[32] H. A. Sauer, Wye-Delta Transfer Standards for Calibration of Wide Range dc Resistance and dc Conductance Bridges. IEEE Trans. Instrum. Meas. **17**, 151-155 (1968).

[33] K. Kupfmuller, Einfiihrung in die theoretische Elektrotechnik. 25-29, Springer, (1968).

[34] R. E. Scott, Linear circuits. 156-169, Addison-Wesley, (1960).

[35] M. Kruskopf, D. M. Pakdehi, K. Pierz, S. Wundrack, R. Stosch, T. Dziomba., M. Götz, J. Baringhaus, J. Aprojanz, and C. Tegenkamp, 2D Mater. **3**, 041002 (2016).

[36] V. Panchal, Y. Yang, G. Cheng, J. Hu, M. Kruskopf, C.-I. Liu, A. F. Rigosi, C. Melios, A. R. Hight Walker, D. B. Newell, O. Kazakova, and R. E. Elmquist, Confocal laser scanning microscopy for rapid optical characterization of graphene. Commun. Phys. **1**, 83 (2018).

[37] M. Kruskopf, A. F. Rigosi, A. R. Panna, M. Marzano, D. Patel, H. Jin, D. B. Newell, and R. E. Elmquist, Next-generation crossover-free quantum Hall arrays with superconducting interconnections. Metrologia **56**, 065002 (2019).

[38] S. Sarkar, H. Zhang, J.-W. Huang, F. Wang, E. Bekyarova, C.N. Lau, and R.C. Haddon, Organometallic hexahapto functionalization of single layer graphene as a route to high mobility graphene devices. Adv. Mater. **25**, 1131 (2013).

[39] A.F. Rigosi, M. Kruskopf, H.M. Hill, H. Jin, B.-Y. Wu, P.E. Johnson, S. Zhang, M. Berilla, A.R. Hight Walker, C.A. Hacker, D.B. Newell, and R.E. Elmquist, Gateless and reversible Carrier density tunability in epitaxial graphene devices functionalized with chromium tricarbonyl. Carbon **142**, 468 (2019).

[40] E. Bekyarova, S. Sarkar, S. Niyogi, M.E. Itkis, and R.C. Haddon, Advances in the chemical modification of epitaxial graphene. J. Phys. D: Appl. Phys. **45**, 154009 (2012).

[41] A.E. Kennelly, Equivalence of triangles and stars in conducting networks. Electrical World and Engineer, **34**, 413–414 (1899).

[42] L. Versfeld, Remarks on Star-Mesh Transformation of Electrical Networks. Electron. Lett. **6**, 597-599 (1970).

[43] A. F. Rigosi, M. Marzano, A. Levy, H. M. Hill, D. K. Patel, M. Kruskopf, H. Jin, R. E. Elmquist, and D.B. Newell, Analytical determination of atypical quantized resistances in graphene pn junctions. Physica B: Condens. Matter **582**, 411971 (2020).

[44] C.-I Liu, D. S. Scaletta, D. K. Patel, M. Kruskopf, A. Levy, H. M. Hill, A. F. Rigosi, Analysing quantized resistance behaviour in graphene Corbino pn junction devices. J. Phys. D: Appl. Phys. **53**, 275301 (2020).